Medical Engineering and Physics 73 (2019) 39–50

Contents lists available at ScienceDirect

Medical Engineering and Physics

journal homepage: www.elsevier.com/locate/medengphy

Data-driven assessment of cardiovascular ageing through multisite photoplethysmography and electrocardiography

Antonio M. Chiarelli[a,*], Francesco Bianco[a,b], David Perpetuini[a], Valentina Bucciarelli[a,b], Chiara Filippini[a], Daniela Cardone[a], Filippo Zappasodi[a], Sabina Gallina[a,b], Arcangelo Merla[a]

[a] Department of Neuroscience and Imaging, Institute for Advanced Biomedical Technologies, University G. D'Annunzio of Chieti-Pescara, Via Luigi Polacchi 13, Chieti 66100, Italy
[b] Institute of Cardiology, University G. D'Annunzio of Chieti-Pescara, Via Dei Vestini 5, 66100, Chieti, Italy

ARTICLE INFO

Article history:
Received 18 April 2019
Revised 11 July 2019
Accepted 18 July 2019

Keywords:
Photoplethysmography (PPG)
Electrocardiography (ECG)
Cardiovascular aging
Arterial stiffness
Deep convolutional neural network (DCNN)

ABSTRACT

The cardiovascular system is designed to distribute a steady flow through its elastic properties. With ageing, fatigue and fracture of elastin lamellae cause a loss of elasticity defined arterial stiffness. Arterial stiffness causes changes of the pulse wave propagation through the arterial tree, which volumetric counterpart can be assessed non-invasively through photoplethysmography (PPG). PPG may be employed in combination with electrocardiography (ECG). It is here reported an implementation of analysis of multisite PPG and single lead ECG relying on Deep Convolutional Neural Networks (DCNNs). DCNNs generate peculiar filters allowing for data-driven automated selection of the features of interest. The ability of a DCNN to predict subject's age from PPG (left and right brachial, radial and tibial arteries plus fingers) and ECG (Lead I) in a healthy male population (age range: 20–70 years) was investigated. A performance in age prediction of 7 years of root mean square error was obtained, which was superior to other feature-based procedures. The accuracy in age prediction of the machinery in the healthy population may serve for the generation of age-matched normal ranges for the identification of outliers suggesting cardiovascular diseases manifesting as fastened cardiovascular ageing which is recognized as a risk factor for ischemic diseases.

1. Introduction

The heart and the arterial tree have the function to deliver blood to capillaries of bodily organs and tissues according to their need. Moreover, the arterial tree cushions the pulse wave generated by the heart allowing for a continuous blood flow [1]. Great emphasis has been placed on the role of arterial aging, as determined by an increased arterial stiffness and loss in the arterial cushion properties. Arterial stiffness is in fact both a marker and an independent risk factor for the development of cardiovascular diseases [2–6]. Although quantitative evaluation of arterial stiffness requires estimating volumetric changes given pressure variations, statistical approaches have been developed to estimate stiffness from its influence on the pulse pressure wave propagation within the arterial tree. In fact, as arteries stiffen with age or disease process, the propagation of the pulse pressure wave from the heart into the arterial tree modifies. It is known that pulse wave velocity (PWV) is monotonically and positively related to arterial stiffness [7,8] since it tends to be proportional to the square root of the incremental elastic modulus of the vessel wall where it propagates [9]. It is generally estimated from measurements performed at two different body locations (e.g., carotid-femoral PWV) with values ranging from 5 m/s in teenagers up to 12 m/s in the old population [10]. When measured at a specific body site, not only the pulse wave time of arrival [11] but also other features of the pulse are sensitive to arterial ageing. With ageing, pulse waveforms transform from a wavy into a more triangular-shaped signals [12]. Although the origin of the pulse shape at different body locations derives from a complex interplay between pulse pressure, arterial stiffness and peripheral resistance, and the contribution of each components is not completely understood, it is generally accepted that pulse shape can provide valuable information about the cardiovascular system status. For example, more than a century ago

Abbreviations: AGI, Ageing Index; ANN, Artificial Neural Network; DCNN, Deep Convolutional Neural Network; DNN, Deep Neural Network; ECG, Electrocardiography; MSE, Mean Squared Error; NIR, Near Infra-Red; OD, Optical Density; PMT, Photo-Multiplier Tube; PPG, Photoplethysmography; PWV, Pulse Wave Velocity; ReLU, Rectified Linear Unit; RMSE, Root Mean Square Error; SNR, Signal to Noise Ratio.

* Corresponding author.
E-mail address: antonio.chiarelli@unich.it (A.M. Chiarelli).

https://doi.org/10.1016/j.medengphy.2019.07.009
1350-4533/

clinicians, using tonometers, measured a rise with ageing in the late systolic component of the pulse measured at the radial artery [13,14].

Photoplethysmography (PPG) [15] is a noninvasive optical technique that exploit near infrared (NIR) light sensitivity to hemoglobin [16], the main absorbing compound in such spectral range, to estimate periodic changes in blood volume within the arteries caused by the pulse pressure wave. Although being a volumetric measure and not a direct measurement of the pulse pressure, thanks to the strict relationship between changes in arterial pressure and volume and its non-invasivity, it is commonly employed for arterial stiffness evaluation. PPG is often performed in a transmission modality on the fingers or toes, allowing the assessment of both arterial oxygen saturation and single wavelength pulse wave contour [17]. Thanks to the high diffusive properties of biological tissues within NIR spectral range [18], PPG measurements can also be performed in a back-reflection modality where the light source and detector are located on the same surface at a certain distance from one another (few centimeters). This procedure allows to investigate larger arteries (e.g., radial and brachial arteries) where transmission modality is not feasible.

PPG signals can be analyzed to retrieve PWV between two different body sites or between the heart and one body site, when employed in combination with ECG recordings, based on the time of arrival of the pulse [11].

The PPG shape contour has been extensively characterized when measured on fingers. It usually is characterized by an early systolic peak and a later peak following a point of inflection that occurs a short time after the first peak in the post-systolic phase. The second peak is supposedly formed by back-reflections at sites of impedance mismatch within the arterial tree and its amplitude and closeness to the early systolic peaks are known to be related to cardiovascular ageing and arterial stiffness [14]. Peaks of PPG contours are generally retrieved by means of PPG first derivative analysis.

Other work was conducted to evaluate PPG pulse shape by means of second derivative analysis (accelerated PPG). A non-linear combination of second derivative values, extracted within the diastolic, systolic and early post-systolic phases of the finger PPG [19], demonstrated good relation with subject's age (correlation between $r = 0.8$ and $r = 0.9$ with an age range of 20–80 years) and was labeled as "ageing index" (AGI) which, to date, provided the best performance in age prediction based on PPG feature analysis [12].

Another approach, alternative to feature extraction by means of derivative analysis, would be to implement data-driven procedures through the employment of advanced machine learning algorithm. In fact, the link between PPG, or PPG and ECG, with subject's age can be conceived as a multivariate regression problem whose transfer function can be learned by artificial intelligence, avoiding a priori feature selection. The only a priori assumption of the procedure (whose assumption can be tested a posteriori) is the existing functional relationship between the input (PPG and ECG) and the output (subject's age). With respect to PPG, such an approach was utilized by Monte-Moreno [20] for prediction of blood glucose and pressure. The relationship between the input and the output has to be learned by the machinery in a supervised learning approach [21].

With respect to supervised learning classification and regression, Artificial Neural Networks (ANNs) are currently showing great potential. ANNs are composed of nonlinear processing units, called neurons. The evolution of ANNs are Deep Neural Networks (DNNs, also labeled as Deep Learning) [22,23]. DNNs are constituted by many layers of neurons and they find complex relationships by minimizing a cost function (a metric of distance between the DNN and real outputs) by means of gradient descent approaches and by using the backpropagation algorithm [24]. Efficient learning algorithms have been implemented to avoid local minima during training and poor generalization (over-fitting) [25] as well as new neuron's activation functions (such as Rectified Linear Unit Function, ReLU function [26]) that dampened the vanishing gradient problem [27]. DNNs can perform very complex, non-linear, regressions and/or classifications, greatly increasing shallow ANN and other machineries performances [28]. DNNs reached incredible classification outcomes when applied to signals and/or to images [29–32], also within the biomedical field [33–35].

A further improvement to DNNs was the implementation of Deep Convolutional Neural Networks (DCNNs). DCNNs are DNNs where neurons are connected to sliding regions of signals and/or images that are close in time and/or space [31,36]. Since neurons of DCNNs are grouped, the parameters of the neurons, because of the learning procedure, generate filters that allow pattern identification with no priors [37].

In this paper investigation of the capabilities of DCNNs for data-driven prediction of the age of healthy adult males as a function of multi-site PPG (left and right brachial, radial and tibial arteries plus fingers) and ECG (Lead I) recordings is reported. The performance of the DCNN was compared to AGI evaluation of the finger PPG and to PPG-ECG feature-based approaches relying on derivative analysis and either on linear or non-linear regressors.

2. Methods

2.1. Participants

25 healthy volunteers, with age ranging from 20 to 70 years (5 participants for each decade, to obtain a uniform age distribution) were enrolled. All participants were male, adults, Caucasian, with no history of cardiovascular, neurological or psychiatric disease; they did not receive medications, nor coffee or energy drinks before the test. All the subjects provided written informed consent, which was performed in agreement with the ethical standards of the Helsinki Declaration, 1964, and approved by the local Human Board Review and Ethical Committee.

2.2. Photoplethysmography (PPG) and electrocardiographic (ECG) recordings

Photoplethysmographic data have been acquired with a multi-channel frequency domain near-infrared (NIR) system (ISS Imagent^{TM}, Champaign, Illinois, Fig. 1(a)). In frequency domain technology, sources are modulated at frequencies of hundreds of megahertz allowing to uncouple and quantitatively evaluate absorption and scattering coefficients of the tissue from signal's amplitude and phase delay measurements [38]. The system was equipped with 32 laser diodes (16 emitting light at 690 nm and 16 at 830 nm) and 4 photo-multiplier tubes (PMTs). Although the instrument recorded light intensity and phase-delay data at two wavelengths, only intensity data at 830 nm of wavelength has been used in the current study, effectively using the system in a single-wavelength, continuous wave (constant source power) modality. In fact, since no quantitative evaluation of tissue absorption and scattering is needed, PPG is generally performed with constant light sources; moreover, the 830 nm wavelength is the color with stronger sensitivity to oxy-hemoglobin, the main oscillating chromophores within the arteries, providing a higher PPG Signal to Noise Ratio compared to 690 nm wavelength [39]. The sampling rate was set at 100 Hz. NIR light was carried to the investigated tissue using optic fibers (0.4 mm core) and from the tissue back to the PMTs using fiber bundles (3 mm diameter). The fibers have

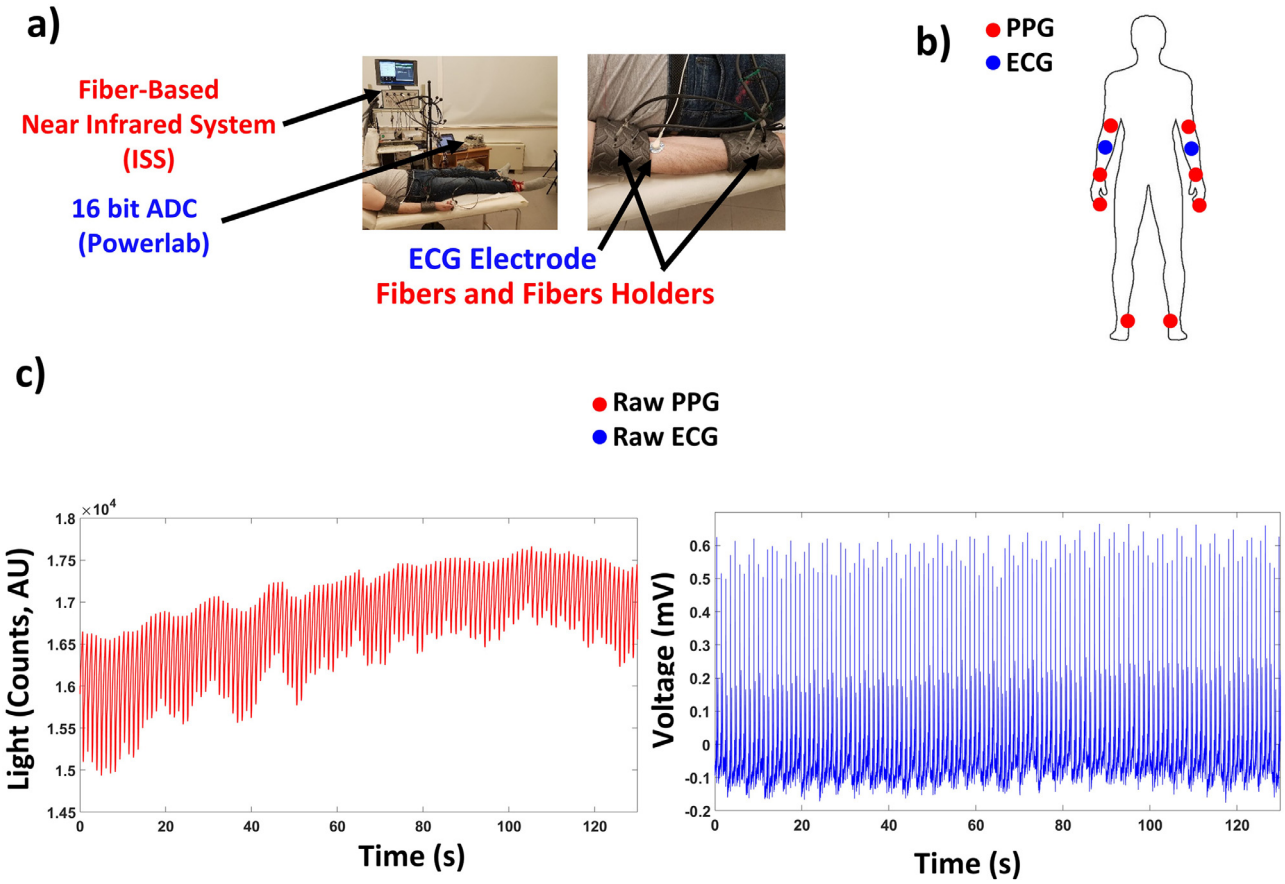

Fig. 1. (a) Experimental setting: PPG was acquired with a multi-channel frequency domain near infrared system (ISS ImagentTM, Champaign, Illinois). NIR light was carried to and from the investigated tissue using optic fibers. The fibers have been held in place using custom-built optical probes; Synchronized ECG was acquired through leads and the analog signals have been sent to a 16-bit Analog to Digital Converter (Powerlab, AD Instruments); during the experiment, the subjects lied supine on a medical cot. (b) 4 PPG channels have been located on the brachial, on the radial and on the tibial arteries as well as on the index. Two recording runs have been performed to investigate both sides of the body. ECG was acquired through single lead ECG recordings (right and left forearm, Lead I). (c) Example of raw PPG signal recorded on the finger for one subject in one run (left image) and raw synchronous Lead 1 ECG signal (right image).

been held in place using custom-built probes. 4 PPG channels have been located on the brachial, on the radial and on the tibial arteries in a back-reflection modality with an inter-optode distance of 2 cm. Notice that, when dealing with a back-reflection recording modality in the NIR spectral range, inter-optode distance affects the investigated depth of the optical probe. Particularly, increasing the inter-optode distance monotonically increases the depth sensitivity of the investigation. Although, thanks to the strong diffusion, the sensitivity of a source-detector pair in a back-reflection modality is an exponentially decaying function of the space investigated [18,40], the maximum depth sensitivity is approximately half of the source-detector distance [41]. Thus, the 2 cm source-detector distance was used to effectively probing tissues at around 1 cm depth from the skin, supposedly being maximally sensitive to the underlying artery investigated.

An additional PPG channel was located on the index finger in a classical transmission modality (Fig. 1(b)).

Synchronized ECG was acquired through single lead ECG recordings (right and left forearm, Lead I, Fig. 1(b)). The analog signals were sent to a 16-bit Analog to Digital Converter (Powerlab, AD Instruments) and sampled at 1 kHz (Fig. 1(a)).

During the experiment, the subjects lay supine on a medical cot (Fig. 1(a)). PPG and ECG data were recorded for 2 min for two different runs. In each run PPG signals were recorded from one side of the body. Within the two runs the PPG probes were moved to the contralateral side. The initial side of recording was randomized among subjects.

2.3. Photoplethysmographic (PPG) and electrocardiographic (ECG) signal pre-processing

Raw PPG signals (Fig. 1(c), left image) have been converted into optical densities (ODs) [42].

Raw PPG OD and ECG (Fig. 1(c), right image) have been filtered with zero-lag 4th order Butterworth digital filters; raw PPG data have been filtered between 0.2 and 10 Hz; raw ECG data have been filtered between 0.2 and 50 Hz (Fig. 2(a) and (b)). One subject was removed due to low quality of filtered signals after visual inspection. A total of 24 subjects were utilized for further analysis.

To identify the R-wave peaks of the ECG, the local maxima were found on a filtered and normalized (z-score) Lead I ECG signals with constraints of a minimum value of the peak of 3, and an interpeak distance of 600 ms.

A visual inspection of the R-wave peaks identification algorithm showed reliable identification performance with a 100% sensitivity and specificity to the R-wave peaks for all the subjects (Fig. 2(b)).

To avoid redundant sampling of PPG and ECG and to homogenize sampling frequency, both signals have been resampled at 50 Hz. Single pulse PPG and ECG signals have been estimated for all channels in a time window from 0.3 s prior to 1.2 s after the R-wave peaks.

The time-window of 1.5 s allowed to encompass a large range of pulsation frequencies (down to a minimum value of 40 beats/min). To account for possible noisy periods of both PPG

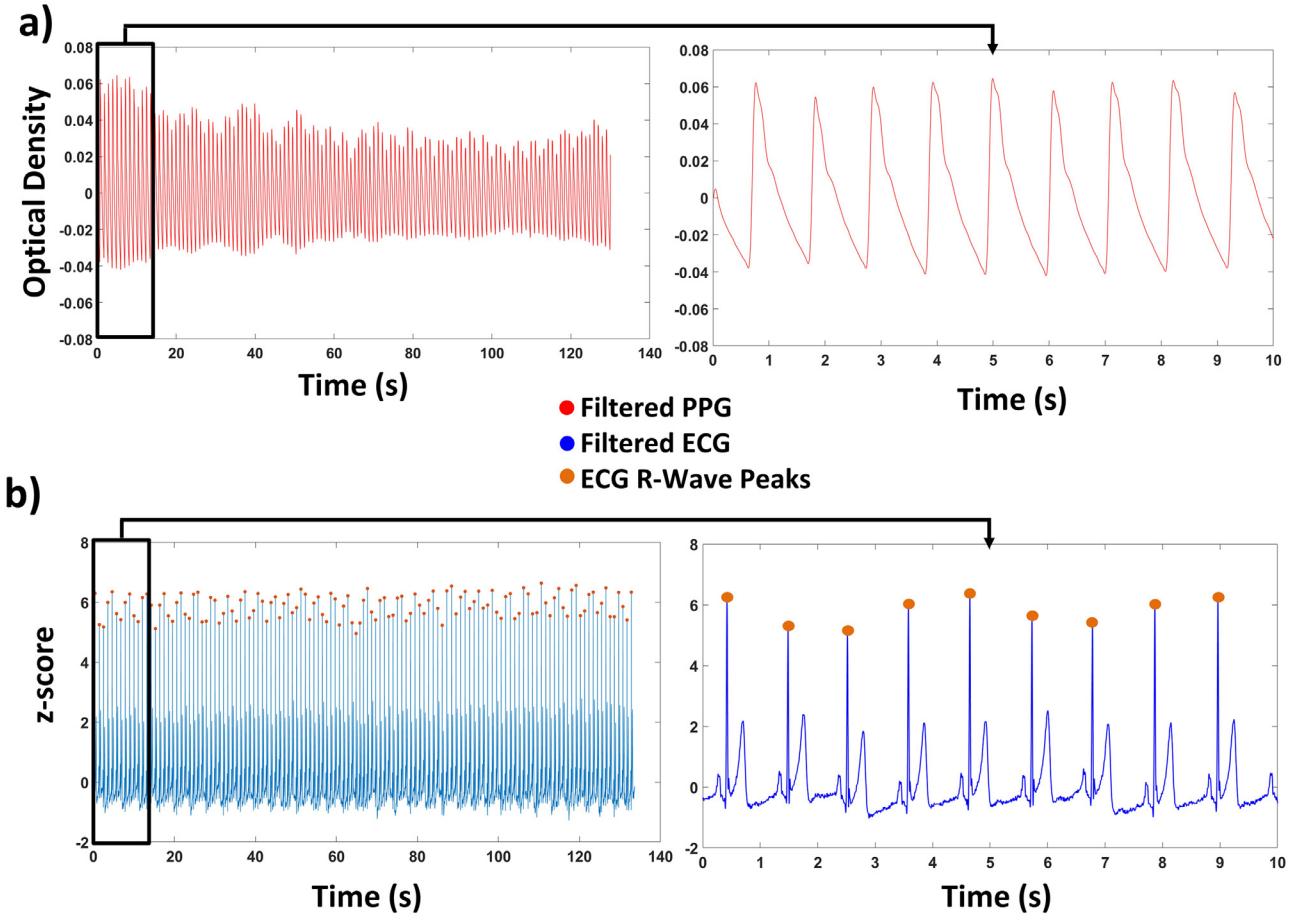

Fig. 2. Example of filtered PPG (a) and ECG (b) recordings for one subject in one run. (b) R-wave peaks of the ECG have been identified through an automated procedure.

and ECG signals, average signals were evaluated with a trim-mean approach by excluding single pulses from the average that had single time-points below or above the 25th or 75th percentile of the sample population. Because of the very high quality of the recorded signals and the low presence of movement artifacts, this analysis ensured a reliable estimate of the pulse average PPG and ECG recordings. An example of pulse average PPG and ECG recordings, together with their standard error (shaded area) showing their small variability, is reported in Fig. 3.

Lead I ECG recordings were averaged between the two runs.

Lead I average ECG and the 8 average PPG recordings have been normalized (z-score) and organized in a time by number of body sites matrices for each of the 24 subjects.

The ages of the subjects have been considered as outputs of the regressors after a normalization process that ensured their values to be constrained between 0 and 1. The normalization decreased the variability of the age variable from STD= 15.4 years to STD=0.335 (dimensionless units).

To increase the data-set numerosity and avoid over-fitting when training, a data-augmentation approach was employed [43]. 99 new input matrices were obtained from each subject by adding noise to the real input coupled with the output age equal to that of the original data. Since we did not want to distort important information while augmenting the data, the new inputs were generated by adding white Gaussian noise to the average and normalized PPG and ECG signals, with a standard deviation of 0.2 (Signal to Noise Ratio, SNR=5). A SNR of 5 was chosen since this value was smaller than the ratio of the diastolic to systolic peaks and the second peak after the inflection point, thus avoiding too much distortion of the after-systolic PPG features.

A total dataset of 2400 inputs (normalized and augmented pulse average multisite PPG and single lead ECG, time by measurement sites matrices) with their respective outputs (normalized ages) were provided to the DCNN or the feature extraction algorithm.

2.4. Deep Convolutional Neural Network (DCNN)

The structure of the DCNN employed in this work was heuristically chosen in similarity with previously reported DCNN structures on biological signal analysis and classification [35]. The structure is reported in Fig. 4(a). The DCNN was composed of 3 convolutional layers and one fully connected layer prior to the output neuron. The input layer was composed of normalized PPG and ECG average signals. The PPG and ECG average signals were $75 \times N$ matrices where 75 is the number of time samples whereas N is the numerosity of the signals employed (PPG at different body sites and *single lead* ECG). The convolutional layers consisted of convolutional (filtering), non-linear and pooling layers performing features extraction and dimension reduction.

For each convolutional layer 10 filters were employed. Since the interest was in creating temporal filters, all filters have been performed in the temporal dimension of the input matrix, and they were of size 6×1 with a stride of 1.

As non-linear function, the Rectified Linear Unit (ReLU) function was employed [26].

For the pooling layer, MaxPooling was utilized, where the largest element from the rectified feature map is retained. A 5×1 MaxPooling was implemented to reduce the dimensionality of each feature to 1 after the three convolutional layers and before the

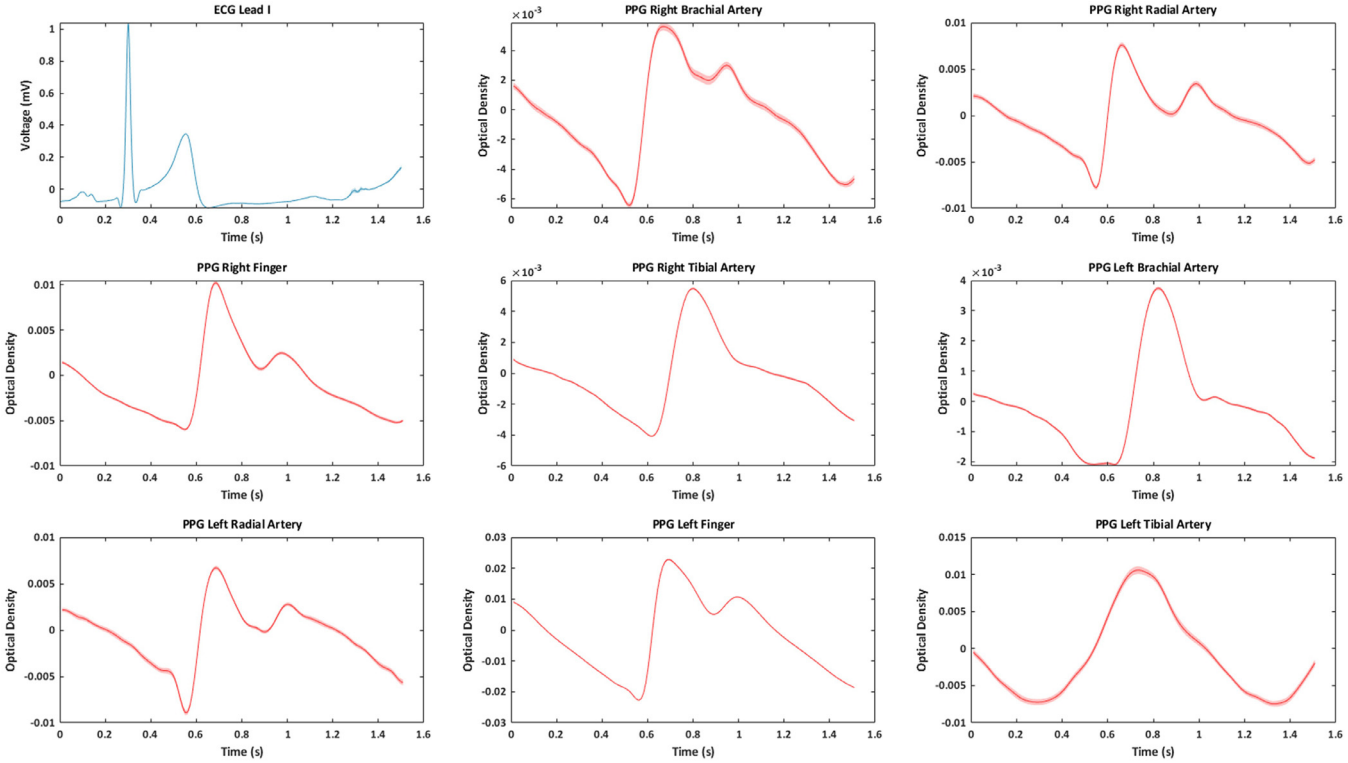

Fig. 3. Example of R-wave locked average Lead I ECG and multisite PPG recordings for one subject (from −0.2 s up to 1.3 s after R-wave, resampled at 50 Hz), together with their standard error (shaded area).

fully connected layer. The fully connected layer (20 neurons performing a ReLU transformation) was introduced to summarize and share information between column of the input matrix (different signals) composed of 10 features each after the last feature extraction layer.

Lastly, a sigmoid function output a value between 0 and 1 predicting the normalized subject's age. All Weights of the DCNN have been initialized in a pseudo-random manner employing a truncated normal distribution (mean=0, standard deviation=0.1, truncation at 2 standard deviations), and the biases have been initialized to 0 [44].

The DCNN was trained in a supervised learning approach [45] by employing the mean squared error (MSE) as objective function and the Adam Optimizer [25] as optimization algorithm. Adam Optimizer parameters were set to: learning rate=10^{-3}, first moment exponential decay rate=$9{\cdot}10^{-1}$, second moment exponential decay rate=$9.99{\cdot}10^{-1}$, constant= 10^{-8} [25].

The optimization procedure was iterated for 1000 epochs with a batch size of 5. A 24-fold cross validation procedure was performed, to address the out-of-training-sample DCNN performance [46]. Since a data augmentation data-set coming from 24 subjects was available for the analysis, each fold was selected from augmented data coming from 1 subject dataset, thus avoiding the presence of data generated from a single subject both in the training and test set.

The described DCNN architecture, training and validation have been implemented in Python through the open-source software library Tensorfow [47]. Further analysis was performed in Matlab.

2.5. Feature-based analysis

A feature extraction algorithm was implemented to extract features of interest from pulse average PPG and ECG signals. For the PPG signals three points of interest have been identified, namely, the diastolic peak, systolic peak, and the first inflection point after the systolic peak (Fig. 5(a)). Diastolic peak and systolic peak have been identified employing a first derivative analysis [14]. Inflection point after the systolic peak was instead estimated as the point of maximum positive value (positive curvature) of the second derivative of the signal after such a peak [19]. For each point of interest 3 features have been selected, namely: time, amplitude and second derivative, for a total of 9 features for each of the 8 PPG location.

For Lead I ECG signal 3 points of interest have been identified through first derivative analysis: P-wave peak, R-wave peak, and T-wave peak and the same 3 features for each point were estimated (time, amplitude and second derivative) (Fig. 5(b)). For combined PPG and ECG estimations a total of 81 features were fed to the regressor (9 features × 9 locations).

As a linear regressor between features and age multiple linear regression was employed [48].

As a non-linear regressor a shallow ANN was implemented, with structure equivalent to the last two layers of the DCNN utilized in the study and trained with an identical procedure to that of the DCNN. The same cross-validation procedure employed for the DCNN was utilized for both the linear and the non-linear feature-based regressions.

2.6. Ageing index (AGI) analysis

The performances of the DCNN and other data-driven feature-based algorithms have been compared to AGI evaluation of PPG measured at the finger location. The algorithm implemented was the one report in the work by Pilt et al. [12]. AGI was estimated for the 24 subjects enrolled by means of second derivative analysis. The PPG was analyzed by using the amplitudes of distinctive peaks of the second derivative "a", "b", "c", "d", and "e", which are situated in the systolic phase of the heart cycle (Fig. 6(a)). AGI was computed as:

$$AGI = \frac{b - c - d - e}{a} \quad (1)$$

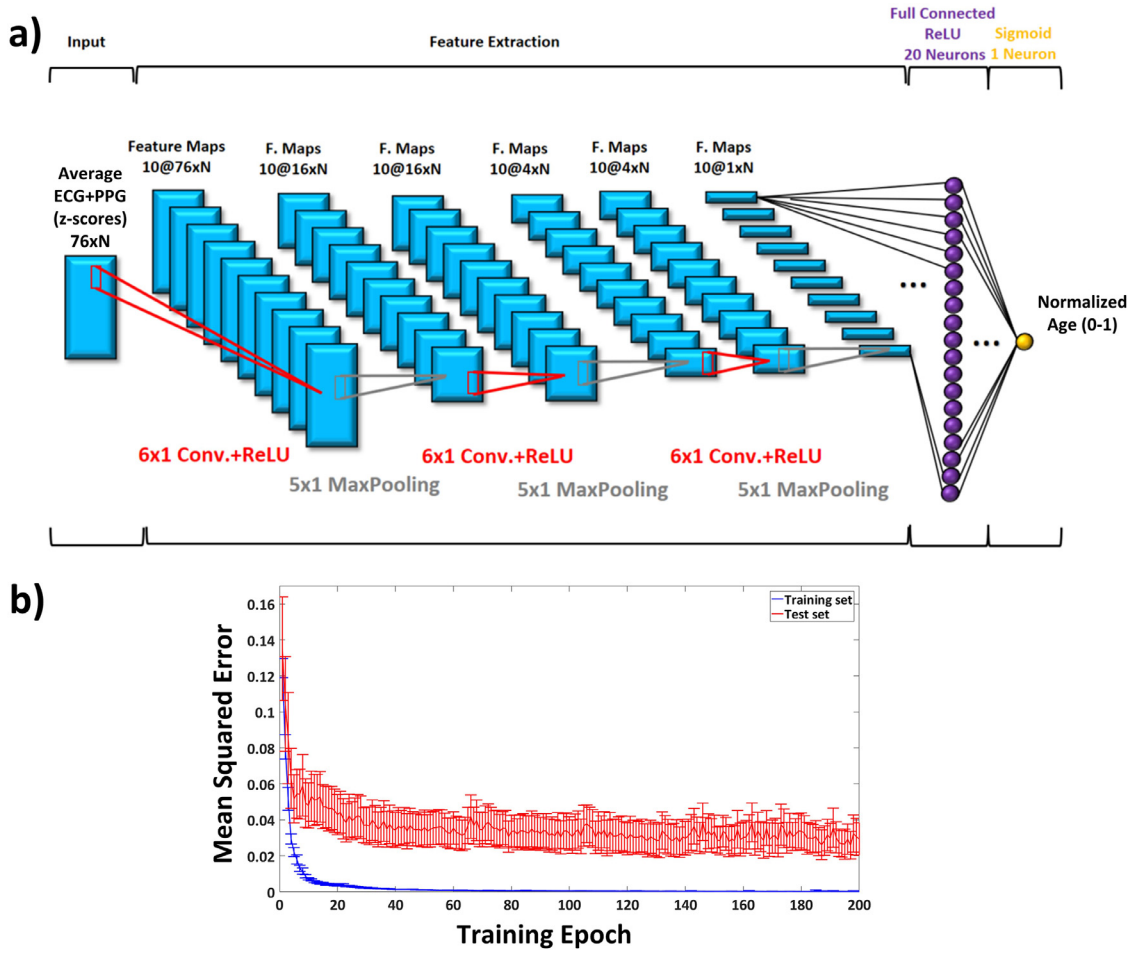

Fig. 4. (a) DCNN employed in the study. The DCNN was composed of 3 convolutional layers, and a fully connected plus a single neuron sigmoid layer. The input layers were composed of normalized PPG and ECG pulse average recordings. The feature extraction section was composed of convolutional, non-linear and pooling layers performing filtering and dimension reduction. The fully connected layer and the sigmoid layer acted as regressor on the features extracted from the convolutional layers (10 features). A one neuron sigmoid layer constituted the output layer to provide predicted subjects' normalized ages based on the inputs. (b) DCNN average (and related standard error) cross-validated objective function (mean squared error between predicted and real normalized age) as a function of the training epoch for the training and the testing set, respectively.

The AGIs of the subject were estimated as the average of right and the left finger PPG outcome.

3. Results

Fig. 6(a) reports an example of AGI estimates based on a second derivative analysis. Fig. 6(b) reports the correlation obtained by evaluating AGI on the finger PPGs as a function of the actual subject's age. A correlation of $r = 0.73$ ($p < 10^{-4}$) was obtained.

The cross-validated, predicted age of the subjects as a function of actual age of the testing set when employing multisite PPG and Lead I ECG recordings in a data-driven fashion are presented in Fig. 7. Of the augmented data-set employed during training and cross-validation, only results obtained from real data are reported. Feature-based analysis results are reported for multiple linear regression (Fig. 7(a)) and shallow ANN (Fig. 7(b)). Feature-less analysis results are reported employing the DCNN (Fig. 7(c)). DCNN averages (and related standard errors) cross-validated MSEs (between predicted and real normalized age) is reported as a function of the training epoch in Fig. 4(b) for training and the testing set. No overfitting effect, increase of the MSE at increasing epoch, is visible in the testing set, proving the efficacy of the data augmentation procedure. For the feature-based analysis and linear regressor, for the feature-based analysis and non-linear regressor and for the DCNN, correlations of $r = 0.64$ ($p < 10^{-3}$), $r = 0.74$ ($p < 10^{-4}$) and $r = 0.92$ ($p < 10^{-9}$) were obtained.

To test the statistical significance of the difference between correlation coefficients of the outputs of the data-driven procedures with age and correlation coefficient between AGI and age, the correlation coefficients were Fisher transformed, and a z test was performed.

Significant increase in correlation with age was obtained when comparing data-driven multisite DCNN to AGI ($Z = 2.14$, $p < 0.05$) whether no difference was found between the feature-based analysis and AGI (Features+Multiple Regression vs. AGI, $Z = -0.55$, $p = N.S.$); Features+Multiple Regression vs. AGI, $Z = 0.07$, $p = N.S.$). Fig. 7(d) reports cross-validated, average (and related standard error) testing-set MSEs as a function of the different multivariate data-driven regressor procedures employed. The estimated root mean square errors (RMSEs), expressed in years, is also reported. Standard errors of the MSEs were estimated employing a Bootstrap procedure [46].

A Friedman Test highlighted a difference in MSE (evaluated on normalized age) depending on the data-driven procedure employed (Chi-Square=15, df = 2, $p < 10^{-3}$). Post-hoc analysis was performed through pairwise comparisons among data-driven approaches relying on Wilcoxon signed rank. Significant differences in MSE were found when comparing feature-less DCNN

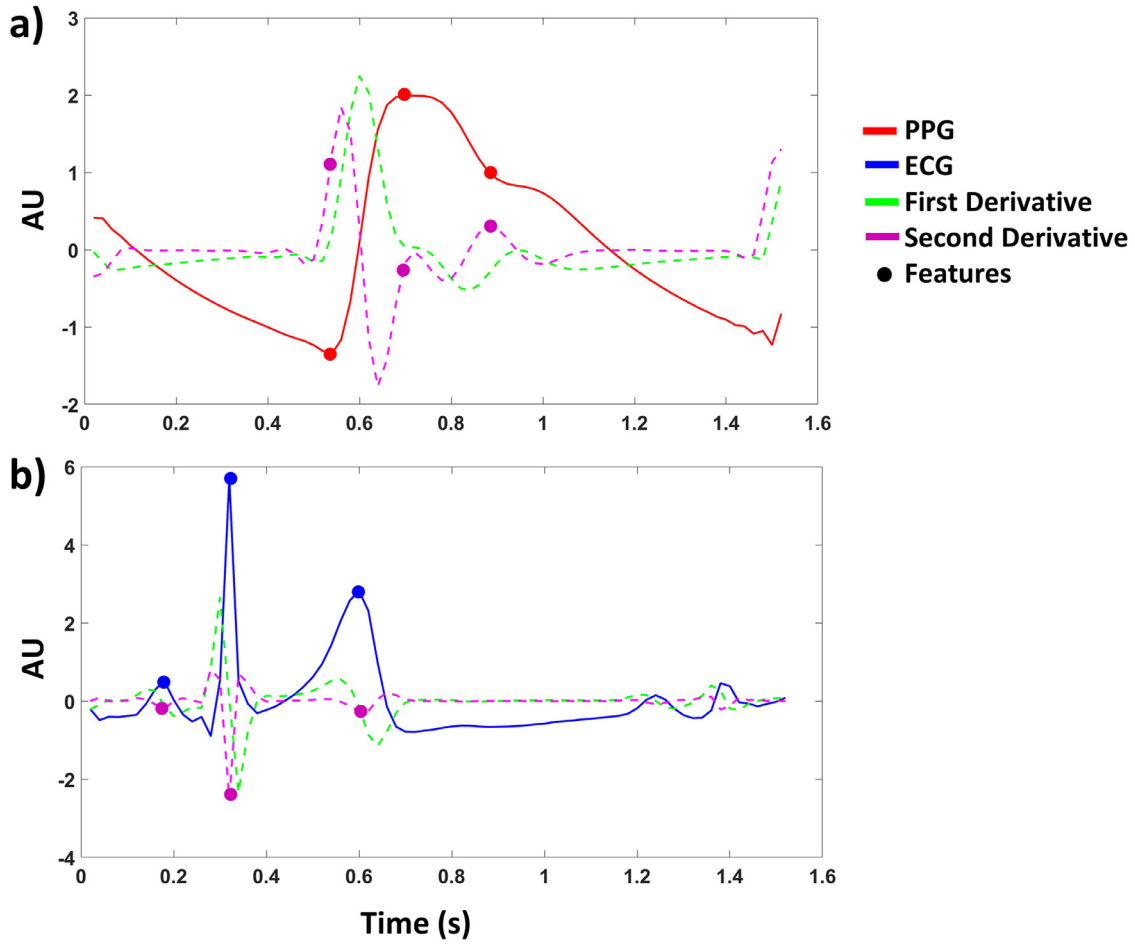

Fig. 5. (a) Example of an average PPG signals and its estimated first and second derivative. 3 points of interest have been identified through derivative analysis: diastolic peak, systolic peak, and inflection point. 9 features have been identified for each PPG waveform, namely, time, amplitude and second derivative of the 3 points. (b) Example of an average ECG signals and its estimated first and second derivative. 3 points of interest have been identified through derivative analysis: P-wave peak, R-wave peak, and T-wave peak. 9 features have been identified for each ECG waveform namely, time, amplitude and second derivative of the 3 points.

analysis (MSE=0.025±0.008) with feature-based analysis (linear, MSE=0.068±0.014 and non-linear regressor, MSE=0.057±0.011) ($Z = -2.97$ $p < 0.01$, $Z = -2.54$, $p < 0.01$). When comparing the two feature-based data-driven multivariate analysis, the non-linear operator performed better than the linear one, however the difference did not reach statistical significance ($Z = -0.083$, $p = 0.4$).

Importantly, when employing the multiple regression analysis, because of its linear nature, it was possible to easily evaluate the impact of each feature in the prediction of the output by analyzing the magnitude of the beta weights (after normalization of both the independent and dependent variables). When averaging the beta weights across features and body sides, we obtained the highest absolute weights on tibial artery PPG (0.044±0.002), followed by Lead I ECG (0.039±0.002), finger PPG (0.038±0.0017) and brachial artery PPG (0.037±0.0013). The smallest absolute weights were associated with measurements performed through radial artery PPG (0.097±0.0008). When evaluating the average weights across locations, we obtained the highest absolute beta weights for time features (0.041±0.002), followed by second derivative features (0.030±0.002) and amplitude features (0.026±0.002).

Furthermore, in order to provide a qualitative analysis of the features extracted by the filters of the DCNN, we divided the subjects by a median split of age and analyzed the different output of the first convolutional layer of the DCNN as a function of the two groups (younger and older subjects). Fig. 8 reports example of this investigatory analysis aiming at highlighting the features extracted by the DCNN to predict age. The figure shows average (and related standard error) input signals and first-convolutional and ReLU layers outputs divided by the median split of age. Fig. 8 reports results for different inputs and the first convolutional layer+ReLU outputs for a particular filter of the first convolutional layer. For ECG Lead I (Fig. 8(a)) the filter seems to highlight age differences of the T-wave, i.e., at the T-wave time there is larger average difference (also when accounting for the standard error of the mean) between the signals of the two groups in the filtered signals compared to the unfiltered ones. In particular, the filter seems to highlight a decreased T-wave peak amplitude in the older population. Fig. 8(b) reports results for the PPG Tibial Artery. This filter seems to highlight age differences in timing of the systolic peak (earlier peak in the older population). Lastly, Fig. 8(c) reports results for the PPG Brachial Artery, highlighting age differences in the post systolic phase of the pulse (with older subjects having smaller curvature in this phase).

Regressors performances when employing PPG at a single body region (utilizing two inputs at the same body regions on the contralateral sites) and Lead I ECG are illustrated in Fig. 9. Single body region PPG and Lead I ECG average (and related standard error) testing-set MSE (evaluated on normalized age) as a function of the locations are displayed for the different regressors. RMSE, expressed in years, is also reported for the smaller and larger MSE retrieved. Best performance (smaller MSE, RMSE) were obtained with PPG measures performed on the tibial artery (MSE=0.055±0.018).

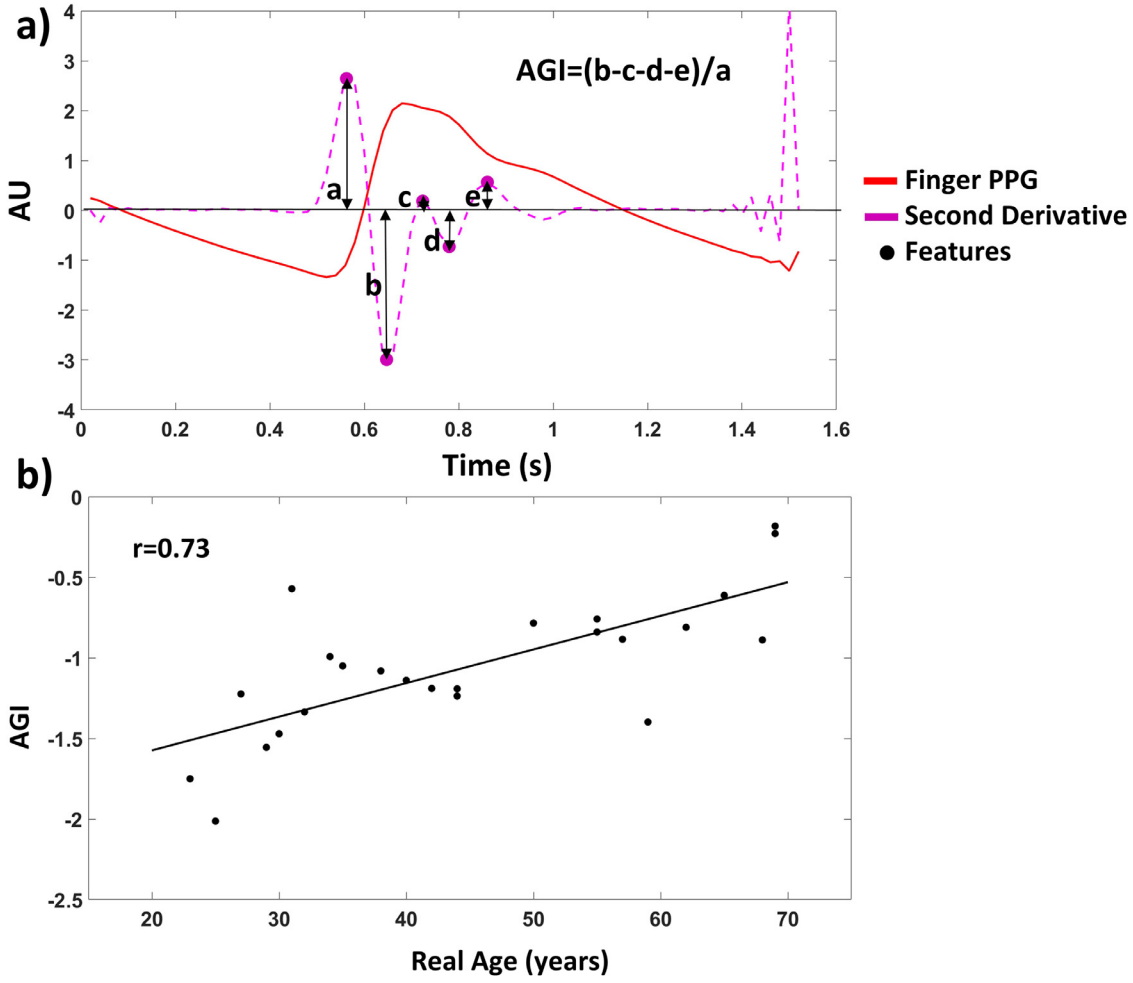

Fig. 6. (a) Example of AGI estimates based on a second derivative analysis. The finger PPG was analyzed by using the amplitudes of distinctive peaks of the second derivative, "a", "b", "c", "d", and "e", which are situated in the systolic phase of the heart cycle. (b) Correlation of AGI as a function of the actual age obtained from the subjects' sample.

However, the obtained MSE was significantly higher than the one obtained employing multimodal and multisite PPG and *Lead I* ECG (MSE=0.025±0.008) ($Z = 1.97$, $p = 0.04$).

4. Discussion

Ageing is accompanied by cardiovascular degradation and arterial stiffness [8]. Several procedures have been developed to predict subject's age relying on measurement of the cardiovascular status through peripheral recordings [11,12]. Accurate age prediction in the healthy population based on peripheral recordings sensitive to cardiovascular ageing may indeed allow the generation of age-matched normal ranges, usable for screening of cardiovascular diseases.

Based on the established sensitivity of PPG and ECG to cardiovascular ageing [8,11,12,49], in this paper we explored the capabilities of combined multisite PPG (left and right brachial, radial and tibial arteries plus fingers) and single site ECG (Lead I) recordings (Figs. 1–3) together with advanced machine learning algorithms (DCNN, Fig. 4) to predict the age of subjects from a healthy male population [50]. The implemented DCNN allowed feature-less PPG and ECG analysis by generating data-driven temporal filters producing an automated selection of signal features sensitive to ageing (Figs. 4 and 8).

DCNN was able to predict the ages of the participants to a high degree of accuracy, with a correlation between real and predicted age of $r = 0.92$, (age range: 20–70 years, Fig. 7(c)) and a RMSE of only 7 years (Fig. 7(d)). This result was compared to more conventional approaches such as AGI computed on finger PPG or on approaches that relied on feature extraction (based on first and second derivative analysis) of the PPG and ECG signals and linear (multiple regression) or non-linear (shallow ANN) regressors. A statistically significant lower accuracy with respect to DCNN in age prediction was obtained with AGI ($r = 0.73$) or utilizing a linear ($r = 0.64$, RMSE=12 years) and non-linear ($r = 0.74$, RMSE 11 years) regressors (Fig. 7(a), (b), and (d)). Although feature-based nonlinear regressor was slightly better performing than AGI and the linear regressor, the differences were not statistically significant. This suggests that the higher performances of DCNN may be more ascribed to its self-selection capabilities of the features of interest rather than the non-linearities involved in the PPG-ECG vs. age regression problem. An investigatory analysis, aiming at highlighting the most evident features extracted by the DCNN in the first convolutional layer of the network, showed DCNN selection of PPG and ECG features such as the timing of the systolic peak in the tibial artery, the curvature of the post systolic phase in the brachial artery and the T-wave peak amplitude of the ECG Lead I. These features are recognized as age-changing characteristics of the PPG and ECG and they have been also evaluated by the feature-based analysis. In particular, PPG timing with respect to the ECG is directly associated to the PWV (and hence elastic properties of arteries) [7] whereas PPG curvature of the post-systolic phase is known to be associated with both PWV and peripheral resistance of distal vessels that cause back-reflections of the propagating pulse wave

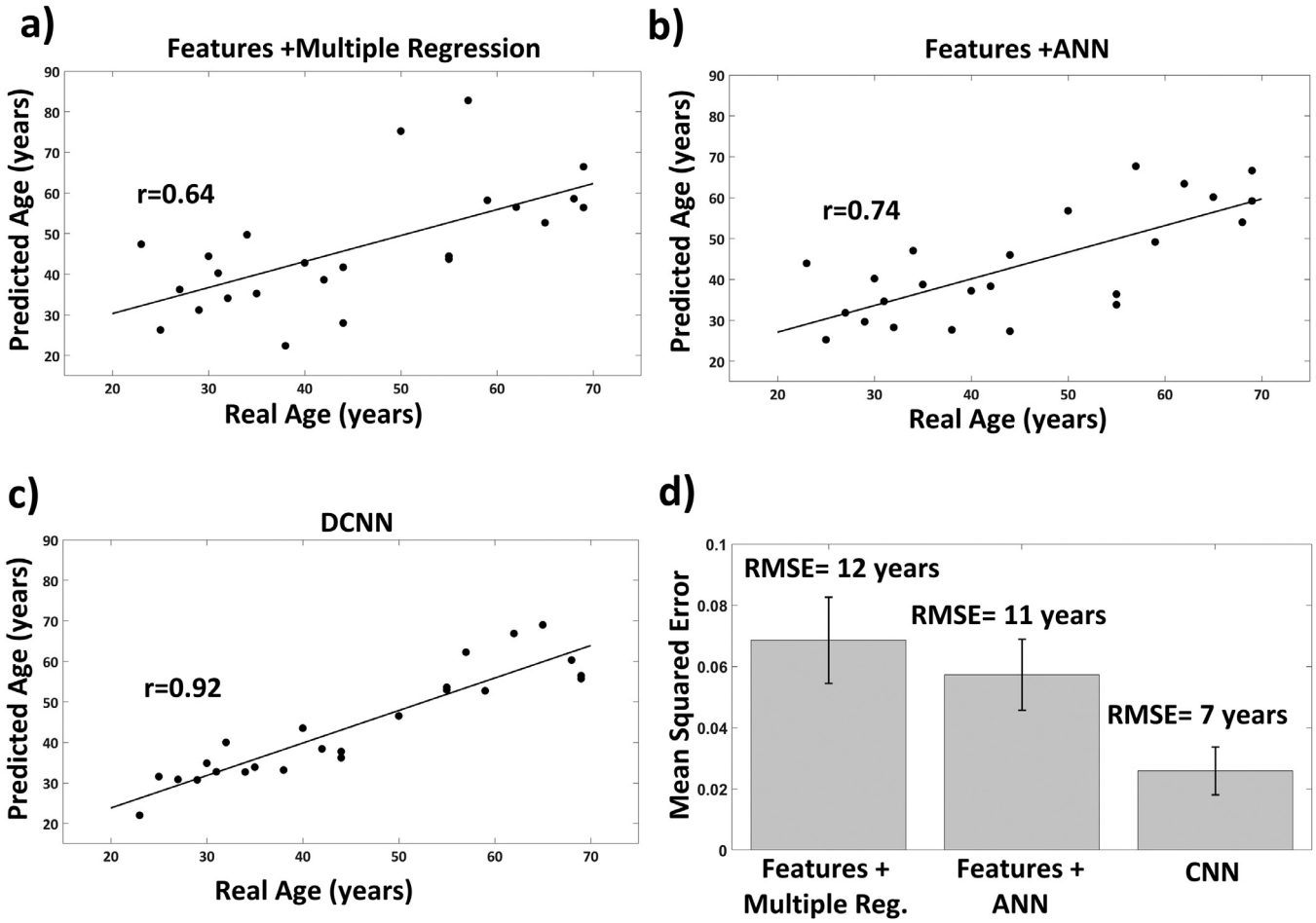

Fig. 7. (a) Predicted subject's age as a function of actual age when employing PPG and ECG features and a multiple linear regression analysis. (b) Predicted subject's age as a function of actual age when employing PPG and ECG features and a shallow ANN. (c) Predicted subject's age as a function of actual age when employing the DCNN on PPG and ECG signals. (d) Cross-validated, average (and related standard error) testing-set mean squared errors (MSEs, evaluated on normalized age) as a function of the different regressor procedures employed. Root mean square errors (RMSEs) expressed in years are also reported.

[51]. Importantly, ECG recordings seemed useful in characterizing cardiovascular ageing beyond the simple triggering of the PPG pulsation analysis. This is depicted from both beta weight evaluation of multiple linear regression (ECG associated beta weights were the second features, after tibial PPG, as assessed by the absolute magnitude of beta weights when employing linear regression in age prediction) and from the qualitative investigation of the effect of DCNN convolutional filters on the input signals (Fig. 8(a)). This means that, by combining ECG with PPG, better performances could be achieved when assessing cardiovascular ageing. The fact that ECG helps in predicting age might be directly associated with arterial stiffness; for example, it has been shown in previous works that arterial stiffness is associated (might induce) cardiac modifications which should reflect in an altered ECG [52]. However, other cardiovascular ageing processes, not directly associated to arterial stiffness, might be the underlying cause of ECG modifications. Indeed, further study, extended to pathological populations, should be conducted to further investigate this aspect.

The higher performances of the DCNN with respect to feature-based procedures could possibly be caused by a lower reliability of the feature extraction algorithm (based on first and second derivative analysis) or to DCNN investigation of less evident signals shape characteristics contributing to the age prediction.

Another important novelty of the proposed work was the evaluation of the PPG signals at multiple body locations. Multisite investigation at different body locations is not particularly common, especially for larger arteries where back-reflection modality is required. For this reason, we compared the multisite recordings with analysis performed employing single body region PPG. Particularly, we evaluated the DCNN and the feature-based algorithms performances when PPG signals, coming from the same contralateral body site, and single lead ECG were provided to the machineries. The best performance in age prediction was obtained when the PPG sensors have been located on the tibial arteries and signals were fed to the DCNN (RMSE=10.8 years). This result might suggest that distal regions can provide higher sensitivity to arterial ageing when estimated using PPG. This result was further corroborated by the multiple linear regression analysis on multisite PPG recordings, where the largest beta weights were associated to PPG features measured on tibial artery. Another possible explanation to the findings is that lower limbs might indeed be more affected by vascular ageing.

Notice that average estimates of PPG and ECG pulsations were examined within a defined time window with respect to the R-wave peak. It should be stressed that the averaging procedure intrinsically does not account for possible single pulsation differences introduced, for example, by the heart rate variability. In fact, this is generally reflected in the slightly larger confidence interval of the retrieved average pulsation before the diastolic peak and in the late post-systolic phase (although the overall small confidence interval of the average pulse, this is slightly appreciable in Fig. 3). Importantly, the diastolic peak location should be stable with

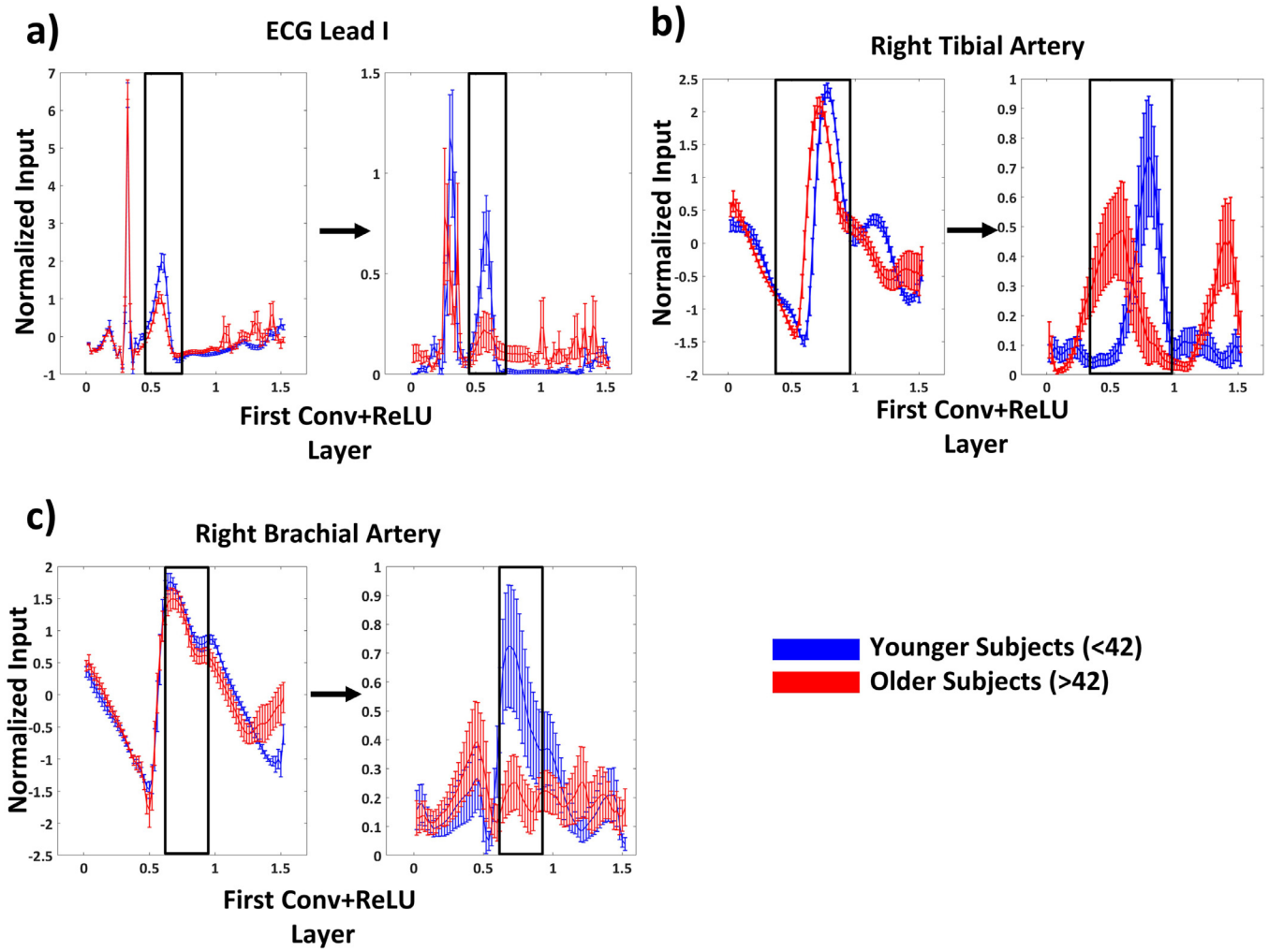

Fig. 8. Example of input signals and first-convolutional and ReLU layers filtered outputs divided by a median split of age. Average values and related standard error are reported for the two groups. (a) ECG Lead I: the first convolutional layer seems to highlight age differences of the T-wave peak. (b) PPG Tibial Artery: the first convolutional layer seems to highlight age differences in timing of the systolic peak. (c) PPG Brachial Artery: the first convolutional layer seems to highlight age differences in the inflection point.

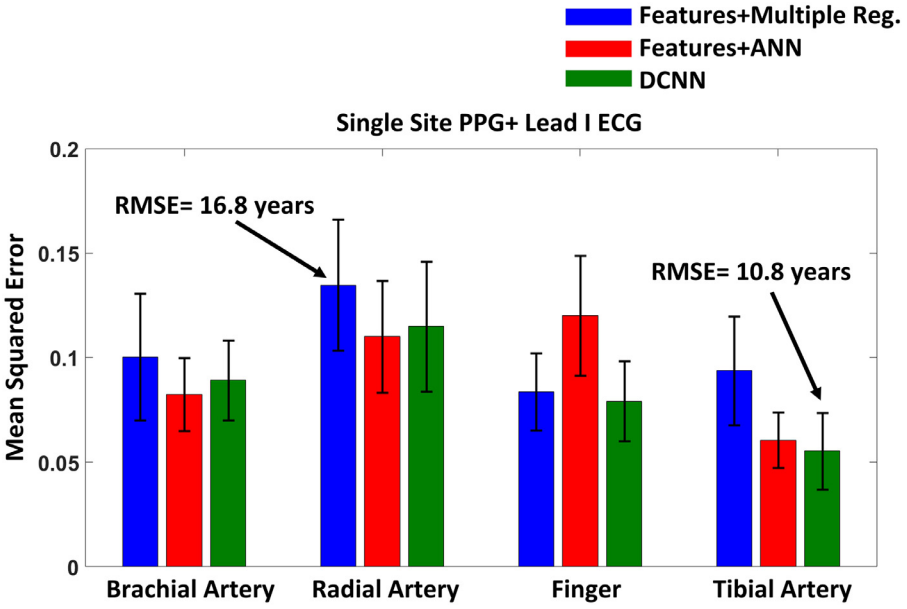

Fig. 9. Lead I ECG and Single PPG site, cross-validated, average (and related standard error) testing-set mean squared error (MSE, evaluated on normalized age) as a function of the locations where measurements were performed for the different regressor employed. Root mean square error (RMSE) expressed in years is also reported for the smallest and largest MSEs (evaluated on normalized age) retrieved.

respect to the R-wave peak, i.e., the average time-of-flight of the pulsation wave should be constant as a function of the heartbeat frequency, avoiding any meaningful signal distortion employing the developed analysis. The larger (unavoidable) variability in the first and in the last part of the averaging period can be shifted at the start or at the end of the evaluation time window by modifying the interval, with respect to the ECG R-wave peak, of the assessment of the average PPG pulse. However, the increased variability in the early diastolic and the late post-systolic phase cannot be avoided through a simple averaging procedure. In fact, the PPG features for the feature-based analysis were selected were the confidence interval was particularly small, i.e., from the diastolic peak to the early post-systolic phase. Possible heart-rate variability effects may be accounted for by employing higher-order statistics (beyond first order analysis, i.e., average) of the single pulses. Although the current work focused on first order (average) analysis of R-wave peak locked average PPG pulsation, a higher order analysis may be conducted in future works.

It should be further stressed that the aim of the study was indeed not age prediction. In fact, there are several procedures to predict age which are more accurate than the PPG-ECG based analysis reported here. However, accurate age prediction based on ECG-PPG, given the PPG-ECG sensitivity to cardiac and vascular status, can be utilized to create narrow normal ranges charts that can be highly sensitive for identifying outliers, thus being indicative of abnormal cardiovascular condition at a given age.

Furthermore, we should comment here that it was explicitly chosen to not include female volunteers in the study. In fact, due to hormonal differences, female cardiovascular status is different than male cardiovascular status [53]. Thus, a different normal range charts should be constructed for such a population (which happens often in medicine, e.g., height or weight charts). We indeed expect in future studies to extend this approach to female population.

The described procedure can provide a cardiovascular related chart which is not only multivariate, but directly a function of the PPG and ECG signals (through the DCNN machinery). The cost of such powerful procedure is indeed the difficult physiological interpretation, i.e. the output is a complex multivariate function of the inputs.

DCNN self-selection of the features of interest in a data-driven manner, generally requires large data-set to avoid over-fitting during training. In this work, since a limited number of subjects were acquired, an augmentation procedure was implemented to dampen the overfitting problem [43]. Although data augmentation seemed to work in dampening overfitting, further research, dealing with combining PPG and ECG recordings with advanced machine learning procedures for estimating arterial stiffness and cardiovascular risk, should indeed focus on increasing the numerosity of the training data-set beyond this study. This would allow to definitely establish age-matched normal ranges. Moreover, similar procedures could be applied to find relation of PPG and ECG characteristics with other cardiovascular risk factors such as hypertension and family history of cardiovascular disease. The proposed algorithm could be also employed as classifier, rather than regressor, to find possible diagnostic and prognostic capabilities when applying the procedure to populations with established cardiovascular diseases.

5. Conclusion

We employed a DCNN in the regression problem of predicting subject's age from pulse average multisite PPG and single lead ECG recordings in a healthy male population (age range: 20–70 years). We obtained accurate age prediction of only 7 years of RMSE, with performances superior to other feature-based approaches. The data-driven self-selected features of the DCNN encompassed several recognized age-changing characteristics of the PPG and ECG ranging from changes in time of PPG systolic peak with respect of the ECG R-wave, shape of the post systolic PPG phase and changes in the ECG T-wave. The demonstrated accuracy in age prediction of the machinery in the healthy population may be useful for generation of age-matched normal ranges and for the assessment of departure from these ranges in vascular diseases.

Combining PPG and ECG recordings with advanced machine learning procedures could also be applied to explore possible relations of PPG and ECG signals with other measurable cardiovascular risk factors. The proposed procedure could be also employed as classifier in populations with established cardiovascular diseases.

Conflict of interest

The authors declare no competing financial and non-financial interests.

Funding

This study was partially funded by grant: 692470, H2020, ECSEL-04-2015-Smart Health, Advancing Smart Optical Imaging and Sensing for Health (ASTONISH).

Ethical approval

Obtained from local Ethical Committee (ID: richijb2l).

References

[1] McDonald's Blood Flow in Arteries. Theoretical, experimental and clinical principles. 6th ed. CRC Press; 2011. https://www.crcpress.com/McDonalds-Blood-Flow-in-Arteries-Sixth-Edition-Theoretical-Experimental/Vlachopoulos-ORourke-Nichols/p/book/9780340985014. (accessed July 2, 2018).

[2] Arnett DK, Evans GW, Riley WA. Arterial stiffness: a new cardiovascular risk factor? Am J Epidemiol 1994;140:669–82. doi:10.1093/oxfordjournals.aje.a117315.

[3] Laurent S, Cockcroft J, Van Bortel L, Boutouyrie P, Giannattasio C, Hayoz D, et al. Expert consensus document on arterial stiffness: methodological issues and clinical applications. Eur Heart J 2006;27:2588–605. doi:10.1093/eurheartj/ehl254.

[4] Mattace-Raso FUS, van der Cammen TJM, Hofman A, van Popele NM, Bos ML, Schalekamp MADH, et al. Arterial stiffness and risk of coronary heart disease and stroke: the Rotterdam study. Circulation 2006;113:657–63. doi:10.1161/CIRCULATIONAHA.105.555235.

[5] Vlachopoulos C, Aznaouridis K, Stefanadis C. Prediction of cardiovascular events and all-cause mortality with arterial stiffness: a systematic review and meta-analysis. J Am Coll Cardiol 2010;55:1318–27. doi:10.1016/j.jacc.2009.10.061.

[6] Yousef Q, Reaz MBI, Ali MaM. The analysis of PPG morphology: investigating the effects of aging on arterial compliance. Meas Sci Rev 2012;12:266–71. doi:10.2478/v10048-012-0036-3.

[7] Hansen TW, Staessen JA, Torp-Pedersen C, Rasmussen S, Thijs L, Ibsen H, et al. Prognostic value of aortic pulse wave velocity as index of arterial stiffness in the general population. Circulation 2006;113:664–70. doi:10.1161/CIRCULATIONAHA.105.579342.

[8] O'Rourke MF, Hashimoto J. Mechanical factors in arterial aging: a clinical perspective. J Am Coll Cardiol 2007;50:1–13. doi:10.1016/j.jacc.2006.12.050.

[9] Anliker M, Moritz WE, Ogden E. Transmission characteristics of axial waves in blood vessels. J Biomech 1968;1:235–46. doi:10.1016/0021-9290(68)90019-5.

[10] Avolio AP, Chen SG, Wang RP, Zhang CL, Li MF, O'Rourke MF. Effects of aging on changing arterial compliance and left ventricular load in a northern Chinese urban community. Circulation 1983;68:50–8. doi:10.1161/01.CIR.68.1.50.

[11] Nitzan M, Khanokh B, Slovik Y. The difference in pulse transit time to the toe and finger measured by photoplethysmography. Physiol Meas 2002;23:85. doi:10.1088/0967-3334/23/1/308.

[12] Pilt K, Ferenets R, Meigas K, Lindberg L-G, Temitski K, Viigimaa M. New photoplethysmographic signal analysis algorithm for arterial stiffness estimation. Sci World J 2013. doi:10.1155/2013/169035.

[13] Mackenzie J. The study of the pulse, arterial, venous and hepatic and of the movements of the heart. J Am Med Assoc 1902(XXXIX):648–9 Edinburgh, UK: Young J Pentland. doi:10.1001/jama.1902.02480370056022.

[14] Kelly R, Hayward C, Avolio A, O'Rourke M. Noninvasive determination of age-related changes in the human arterial pulse. Circulation 1989;80:1652–9. doi:10.1161/01.CIR.80.6.1652.

[15] Allen J. Photoplethysmography and its application in clinical physiological measurement. Physiol Meas 2007;28:R1. doi:10.1088/0967-3334/28/3/R01.

[16] Mancini DM, Bolinger L, Li H, Kendrick K, Chance B, Wilson JR. Validation of near-infrared spectroscopy in humans. J Appl Physiol 1994;77:2740–7. doi:10.1152/jappl.1994.77.6.2740.
[17] Rusch TL, Sankar R, Scharf JE. Signal processing methods for pulse oximetry. Comput Biol Med 1996;26:143–59. doi:10.1016/0010-4825(95)00049-6.
[18] Chiarelli AM, Maclin EL, Low KA, Mathewson KE, Fabiani M, Gratton G. Combining energy and Laplacian regularization to accurately retrieve the depth of brain activity of diffuse optical tomographic data. J Biomed Opt 2016;21:36008. doi:10.1117/1.JBO.21.3.036008.
[19] Takazawa K, Tanaka N, Fujita M, Matsuoka O, Saiki T, Aikawa M, et al. Assessment of vasoactive agents and vascular aging by the second derivative of photoplethysmogram waveform. Hypertension 1998;32:365–70. doi:10.1161/01.HYP.32.2.365.
[20] Monte-Moreno E. Non-invasive estimate of blood glucose and blood pressure from a photoplethysmograph by means of machine learning techniques. Artif Intell Med 2011;53:127–38. doi:10.1016/j.artmed.2011.05.001.
[21] Nasrabadi NM. Pattern recognition and machine learning. J Electron Imaging 2007;16:049901. doi:10.1117/1.2819119.
[22] Bianchini M, Scarselli F. On the complexity of neural network classifiers: a comparison between shallow and deep architectures. IEEE Trans Neural Netw Learn Syst 2014;25:1553–65. doi:10.1109/TNNLS.2013.2293637.
[23] LeCun Y, Bengio Y, Hinton G. Deep learning. Nature 2015;521:436–44. doi:10.1038/nature14539.
[24] Hecht-Nielsen R. III3 – Theory of the backpropagation neural network*. In: Wechsler H, editor. Proceedings of the 1992 International Joint Conference on Neural Networks. Academic Press; 1992. p. 65–93. doi:10.1016/B978-0-12-741252-8.50010-8.
[25] Kingma DP, Ba J. Adam: a method for stochastic optimization. ArXiv:14126980 Cs 2014.
[26] Maas AL, Hannun AY, Ng AY. Rectifier nonlinearities improve neural network acoustic models. In: Proc. icml, 30; 2013. p. 3.
[27] Pascanu R, Mikolov T, Bengio Y. On the difficulty of training recurrent neural networks. ArXiv:12115063 Cs 2012.
[28] Chiarelli AM, Croce P, Merla A, Zappasodi F. Deep learning for hybrid EEG-fNIRS brain–computer interface: application to motor imagery classification. J Neural Eng 2018;15:036028.
[29] Collobert R, Weston J. A unified architecture for natural language processing: deep neural networks with multitask learning. In: Proceedings of the twenty-fifth international conference on machine learning. ACM; 2008. p. 160–7. doi:10.1145/1390156.1390177.
[30] Hinton G, Deng L, Yu D, Dahl GE, Mohamed Ar, Jaitly N, et al. Deep neural networks for acoustic modeling in speech recognition: the shared views of four research groups. IEEE Signal Process Mag 2012;29:82–97. doi:10.1109/MSP.2012.2205597.
[31] Krizhevsky A, Sutskever I, Hinton GE. ImageNet classification with deep convolutional neural networks. In: Pereira F, Burges CJC, Bottou L, Weinberger KQ, editors. Advances in neural information processing systems, 25. Curran Associates, Inc.; 2012. p. 1097–105.
[32] Simonyan K, Zisserman A. Very deep convolutional networks for large-scale image recognition. ArXiv:14091556 Cs 2014.
[33] Ciresan D, Giusti A, Gambardella LM, Schmidhuber J. Deep neural networks segment neuronal membranes in electron microscopy images. In: Pereira F, Burges CJC, Bottou L, Weinberger KQ, editors. Advances in neural information processing systems, 25. Curran Associates, Inc.; 2012. p. 2843–51.
[34] Ronneberger O, Fischer P, Brox T. U-Net: convolutional networks for biomedical image segmentation. ArXiv:150504597 Cs 2015.
[35] Croce P, Zappasodi F, Marzetti L, Merla A, Pizzela V, Chiarelli AM. Deep convolutional neural networks for feature-less automatic classification of independent components in multi-channel electrophysiological brain recordings. IEEE Trans Biomed Eng 2018 1–1. doi:10.1109/TBME.2018.2889512.
[36] Kalchbrenner N, Grefenstette E, Blunsom P. A convolutional neural network for modelling sentences. ArXiv:14042188 Cs 2014.
[37] Esteva A, Kuprel B, Novoa RA, Ko J, Swetter SM, Blau HM, et al. Dermatologist-level classification of skin cancer with deep neural networks. Nature 2017;542:115–18. doi:10.1038/nature21056.
[38] Chiarelli AM, Maclin EL, Low KA, Fantini S, Fabiani M, Gratton G. Low-resolution mapping of the effective attenuation coefficient of the human head: a multidistance approach applied to high-density optical recordings. Neurophotonics 2017;4:021103. doi:10.1117/1.NPh.4.2.021103.
[39] Zijlstra WG, Buursma A, Meeuwsen-van der Roest WP. Absorption spectra of human fetal and adult oxyhemoglobin, de-oxyhemoglobin, carboxyhemoglobin, and methemoglobin. Clin Chem 1991;37:1633–8.
[40] Chiarelli AM, Zappasodi F, Pompeo FD, Merla A. Simultaneous functional near-infrared spectroscopy and electroencephalography for monitoring of human brain activity and oxygenation: a review. Neurophotonics 2017;4:041411. doi:10.1117/1.NPh.4.4.041411.
[41] Harris DNF, Cowans FM, Wertheim DA, Hamid S. NIRS in adults – effects of increasing optode separation. In: Vaupel P, Zander R, Bruley DF, editors. Oxygen transport to tissue XV. Boston, MA: Springer US; 1994. p. 837–40. doi:10.1007/978-1-4615-2468-7_109.
[42] Chiarelli AM, Libertino S, Zappasodi F, Mazzillo MC, Pompeo FD, Merla A, et al. Characterization of a fiber-less, multichannel optical probe for continuous wave functional near-infrared spectroscopy based on silicon photomultipliers detectors: in-vivo assessment of primary sensorimotor response. Neurophotonics 2017;4:035002. doi:10.1117/1.NPh.4.3.035002.
[43] Witten IH, Frank E, Hall MA, Pal CJ. Data mining: practical machine learning tools and techniques. Morgan Kaufmann; 2016.
[44] Sutskever I, Martens J, Dahl G, Hinton G. In: On the importance of initialization and momentum in deep learning; 2013. p. 1139–47.
[45] Hastie T, Tibshirani R, Friedman J. The elements of statistical learning: data mining, inference, and prediction. 2nd ed. New York: Springer-Verlag; 2009.
[46] Kohavi R. A study of cross-validation and bootstrap for accuracy estimation and model selection. In: Proceedings of the fourteenth international joint conference on artificial intelligence – Vol. 2. Morgan Kaufmann Publishers Inc.; 1995. p. 1137–43.
[47] Abadi M, Agarwal A, Barham P, Brevdo E, Chen Z, Citro C, et al. TensorFlow: large-scale machine learning on heterogeneous distributed systems. ArXiv:160304467 Cs 2016.
[48] Johnson RA, Wichern DW. Multivariate analysis. Encycl Stat Sci 2006 American Cancer Society. doi:10.1002/0471667196.ess6094.
[49] Boyd AC, Richards DAB, Marwick T, Thomas L. Atrial strain rate is a sensitive measure of alterations in atrial phasic function in healthy ageing. Heart 2011;97:1513–19. doi:10.1136/heartjnl-2011-300134.
[50] Möller-Leimkühler AM. Gender differences in cardiovascular disease and comorbid depression. Dialogues Clin Neurosci 2007;9:71–83.
[51] McEniery CM, Yasmin, Hall IR, Qasem A, Wilkinson IB, Cockcroft JR, et al. Normal vascular aging: differential effects on wave reflection and aortic pulse wave velocity: the anglo-cardiff collaborative trial (ACCT). J Am Coll Cardiol 2005;46:1753–60. doi:10.1016/j.jacc.2005.07.037.
[52] Hsu P-C, Tsai W-C, Lin T-H, Su H-M, Voon W-C, Lai W-T, et al. Association of arterial stiffness and electrocardiography-determined left ventricular hypertrophy with left ventricular diastolic dysfunction. PLoS One 2012;7. doi:10.1371/journal.pone.0049100.
[53] Rossouw JE. Hormones, genetic factors, and gender differences in cardiovascular disease. Cardiovasc Res 2002;53:550–7. doi:10.1016/S0008-6363(01)00478-3.